



Discovery of novel $\alpha 7$ nicotinic acetylcholine receptor ligands via pharmacophoric and docking studies of benzylidene anabaseine analogs

David C. Kombo*, Anatoly A. Mazurov, Joseph Chewning, Philip S. Hammond, Kartik Tallapragada, Terry A. Hauser, Jason Speake, Daniel Yohannes, William S. Caldwell

Targacept Inc., 200 East First Street, Suite 300, Winston-Salem, NC 27101 4165, USA

ARTICLE INFO

Article history:

Received 3 September 2011

Revised 18 November 2011

Accepted 21 November 2011

Available online 30 November 2011

Keywords:

AChBPs

Nicotinic acetylcholine receptor $\alpha 7$

Pharmacophore

Docking

Benzylidene anabaseine analogs

Spirodiazepine and spiroimidazoline quinuclidine series

ABSTRACT

Based on pharmacophore elucidation and docking studies on interactions of benzylidene anabaseine analogs with AChBPs and $\alpha 7$ nAChR, novel spirodiazepine and spiroimidazoline quinuclidine series have been designed. Binding studies revealed that some of hydrogen-bond donor containing compounds exhibit improved affinity and selectivity for the $\alpha 7$ nAChR subtype in comparison with most potent metabolite of GTS-21, 3-(4-hydroxy-2-methoxybenzylidene)-anabaseine. Hydrophobicity and rigidity of the ligand also contribute into its binding affinity. We also describe alternative pharmacophoric features equidistant from the carbonyl oxygen atom of the conserved Trp-148 of the principal face, which may be exploited to further design diverse focused libraries targeting the $\alpha 7$ nAChR.

© 2011 Elsevier Ltd. All rights reserved.

Neuronal nicotinic acetylcholine receptors (nAChR) are pentameric ligand-gated ion channels of broad distribution and structural heterogeneity. Such diversity in both function and distribution indicates involvement in a variety of neuronal processes and has generated great interest in these acetylcholine receptors as targets for therapeutic intervention in a number of pathological conditions and diseases.¹ The $\alpha 7$ subtype (a homopentamer consisting of five $\alpha 7$ subunits) has been extensively studied in recent years. The human $\alpha 7$ subunit is approximately 50 kD in size and composed of 502 amino acids, including a 22 amino acid signal peptide. The protein may be divided into an extracellular N-terminal and a transmembrane domains. The N-terminal domain, composed of approximately 200 amino acids forming ten β strands, encompasses the ligand-binding domain. The transmembrane domain comprises four α helices crossing the lipid bi-layer and constitutes the ion channel. The $\alpha 7$ nAChR is highly permeable to Ca^{2+} ions, and is therefore characterized as a calcium channel. Agonist binding leads to conformational changes via a quaternary symmetrical twist, opening the hydrophobic gate and allowing passage of ions.

Subsequent to activation, the $\alpha 7$ nAChR rearranges into desensitized state resulting in loss of biological response.²

The $\alpha 7$ subunit is expressed at high levels in hippocampus and cerebral cortex, brain regions involved in learning and memory.³ Accumulating physiological,⁴ pharmacological,⁵ and human genetic⁶ experimental data suggest involvement of $\alpha 7$ nAChR in the cognitive deficits associated with a number of neuropsychiatric and neurodegenerative diseases including schizophrenia and Alzheimer's disease. The growing body of evidence has highlighted the clinical need for the development of $\alpha 7$ nAChR agonists, which may offer new approaches to the treatment of impaired cognitive functions.

Acetylcholine-binding protein (AChBP) folds into a homopentameric structure similar to the extracellular ligand-binding domain of $\alpha 7$ nAChR. Several crystal structures of AChBPs and their variants, in complex with nicotinic ligands have been solved.^{7–12} These structural biology studies have shown that the molecular recognition process between ligands and nAChRs primarily occurs through cation– π interactions, hydrogen-bonding interactions, π – π and hydrophobic interactions as well.^{13–15} Ulens et al.¹⁶ have recently shown that an AChBP crystal structure could be used as a surrogate for docking, in attempt to identify novel $\alpha 7$ nAChR ligands. Prior to this, Taylor and co-workers have also used AChBP crystal structures to rationalize the binding mode of agonists to the $\alpha 7$ nAChR.¹² Benzylidene anabaseine analogs exhibit functional selectivity towards $\alpha 7$ nAChR^{17,18} with the 4-hydroxy-containing

Abbreviations: AChBP, acetylcholine-binding protein; DMXBA, 3-(2,4-dimethoxybenzylidene)-anabaseine; HBD, hydrogen-bond donor; nAChR, nicotinic acetylcholine receptor; Pdb, protein databank; rmsd, root-mean-squared-deviation; ROC, receiver operating characteristic curve.

* Corresponding author. Tel.: +1 336 480 2127; fax: +1 336 480 2107.

E-mail address: david.kombo@targacept.com (D.C. Kombo).

derivatives being among the most potent of this congeneric series. Crystallographic studies of the 3-(4-hydroxy-2-methoxybenzylidene)-anabaseine (**1a**) a metabolite of 3-(2,4-dimethoxybenzylidene)-anabaseine (GTS-21, **1b**), in complexation with *Aplysia* AChBP have shown that its OH group forms a hydrogen-bond to a polar side chain triad made of Asp-164, Ser-166 and Ser-167, which are all located in loop F.¹² Using docking, and comparative modeling, we found that a similar hydrogen-bond donor (HBD) contributes to the interaction of these ligands with *Bulinus* AChBP and the $\alpha 7$ nAChR, whereas in the case of *Lymnaea*, the ligand OH group acts as a hydrogen bond acceptor instead, and interacts with Gln-73 of the complementary face.

Pharmacophore elucidation studies were carried out to explore quantitative 3D QSAR models to predict AChBP K_d and $\alpha 7$ nAChR K_i , as described herein.¹⁹ Summary statistics for the best model derived in each case are shown in Table 1 and indicate that based on Pearson's correlation coefficient and root-mean-square-deviation, derived models show reasonable ability to predict binding. The results obtained for the best 10 pharmacophore hypotheses indicate that the most frequent chemical features observed were positive charge, hydrogen-bond donor, hydrogen-bond acceptor, ring aromatic and hydrophobic. Fischer randomization tests for each pharmacophore model were carried out to demonstrate that correlations observed between the predicted biological activity and ligand molecular descriptors did not result from chance correlation. In each case, K_d or K_i values were scrambled nine times; random models were generated and compared to their non-random counterpart. The significance thus derived for the best models were 90%, for Bt, Ls, and $\alpha 7$, and 70% for Ac. The enrichment obtained when screening a diverse library for rat $\alpha 7$ binding is 2.70, 1.75, 1.47, and 1.44 for the best model derived from Ac, rat $\alpha 7$, Bt, and Ls, respectively. The average distance constraint between the minimum value of 1.97 Å and maximum value of 9.30 Å obtained is about 5.6 Å.

Figure 1 illustrates mapping of compounds **1a** and **1b** onto the best pharmacophore models for each AChBP and the $\alpha 7$ nAChR. We find that the ranked order of fitness to the pharmacophore hypotheses and predicted K_d values for both compounds, for all three AChBP models, is consistent with the trend in experimentally-determined K_d values. Likewise, the ranked order of fitness to the pharmacophore hypothesis and predicted K_i values for both compounds, for the rat $\alpha 7$ nAChR model, is consistent with the ranked order of experimentally-determined K_i values. Taken together, these results suggest that binding of anabaseine analogs to these four proteins is mediated by cation- π , π - π , hydrophobic and hydrogen-bonding interactions, which is in agreement with the well-known nicotinic ligands pharmacophore,¹ as well as docking studies (Figs. 2–5), and co-crystallographic data.

We have designed novel HBD-containing spirodiazepine and spiroimidazoline series (Scheme 1), as ligands aimed at interacting with the $\alpha 7$ nAChR. Our underlying reasoning was that quinuclidine analogs containing a HBD functional group separated from

the cationic center by a distance approximately equal to the average distance constraint required for binding to rat $\alpha 7$, Ac, Bt, or Ls (about 5.6 Å), could theoretically satisfy the docking-derived receptor-based pharmacophoric distance (approximately 12.9 Å) required for binding to the $\alpha 7$ nAChR, as shown in Figure 2a. One should note that in addition to the mere ligand HBD-cation distance, the length of the N–H bond (1.01 Å), O–H bond (0.95 Å), and twice the optimum hydrogen-bond distance (~ 2.5 Å), should be taken into account. The binding affinity of the designed library of spirodiazepine and spiroimidazoline quinuclidines to rat $\alpha 7$ nAChR was predicted using pharmacophore models and molecular docking as described herein.²⁰ Scheme 1 shows the synthetic scheme of the compounds made.

Compounds containing hydroxyl group (**2a–g**, **3a**) or amino group (**3b**) as a hydrogen bond donor have been synthesized by coupling 3-amino-3-(aminomethyl)quinuclidine (**4**) with series of aroylacates,²¹ methyl 2-(cyanomethoxy)benzoate or (2-cyanophenoxy)acetonitrile. Spirodiazepine **2h** without hydroxyl moiety has been obtained by condensation of diamine **1** with [3-(dimethylamino)-2-phenylprop-2-enylidene]-dimethylammonium hexafluorophosphate. Heating in a microwave of diamine **1** with diethyl 2-phenylmalonate or methyl benzimidate provided 1,4-diazepindione **2i** and phenylimidazoline **3c**. Hydroxyphenylimidazoline **3d** has been carried out by cyclization of 3-amino-3-(aminomethyl)quinuclidine (**1**) with 2-(2-hydroxyphenyl)-1,3-benzoxazin-4-one.²²

The experimentally observed binding data²³ obtained for the designed compounds are shown in Table 2. Results show that none of the designed compounds interact with the $\alpha 4\beta 2$ nAChR. Furthermore, none of the designed compounds exhibited binding neither to the ganglion-type $\alpha 3\beta 4$ nAChR nor to muscle-type nicotinic receptors. HBD-containing compounds **3a**, **3b** and **3d**, interact with $\alpha 7$ nAChR with $K_i < 300$ nM likewise, compounds **2a** through **2g**, which might tautomerize into lactim,²⁴ interact with the $\alpha 7$ subtype. All active compounds exhibit a HBD-cation distance within the longest range of 5.47–7.65 Å. Substitution within the aromatic ring of compounds **2a–g** slightly affects interaction with the receptor, while potential conjugation of the aromatic ring and azomethine moiety provide π - π interactions. However, compound **2i**, which might also tautomerize into lactim does not interact with the rat $\alpha 7$ receptor. Although this compound satisfies the distance requirement like its counterparts **2a–g**, it exhibits reduced conjugation pattern and as a result, its tautomeric forms are the most polar of the series, as expressed by their AlogP98 values (–2.33 and –3.74), which are the lowest in the series, as shown in Table 2. A similar trend was also observed when logD at pH 7.4 was used instead of AlogP98 (data not shown). Reduced conjugation and high polarity prevent the compound to interact with the hydrophobic and aromatic rings in the protein binding site, while such interactions have been shown to be important both by ligand-based pharmacophore modeling (Fig. 1 and Table 1) and receptor structure-based docking studies described herein. On the whole,

Table 1
Summary statistics of the best ligand-based pharmacophore models

Pharmacophore model	<i>r</i>	rmsd	Confidence level (%)	Chemical features	Distance constraint HBD-positive charge (Å)	Enrichment factor
Ac	0.77	1.02	70	HBA, HBD, positive charge & hydrophobic	7.46–8.46	2.70
Bt	0.69	0.99	90	HBD & positive	1.97–3.97	1.47
Ls	0.62	1.27	90	HBA, HBD & positive charge	4.23–6.23	1.44
$\alpha 7$	0.70	0.66	90	HBD, ring aromatic & positive charge	7.30–9.30	1.75

The parameter *r* designates the Pearson correlation coefficient between the observed and predicted K_d (or K_i) values, rmsd designates the root-mean-squared-deviation between observed and predicted K_d (or K_i) values. HBA and HBD designate hydrogen-bond acceptor and hydrogen-bond donor, respectively. The enrichment factor was calculated using a test set of 493 diverse compounds, as described in methods.

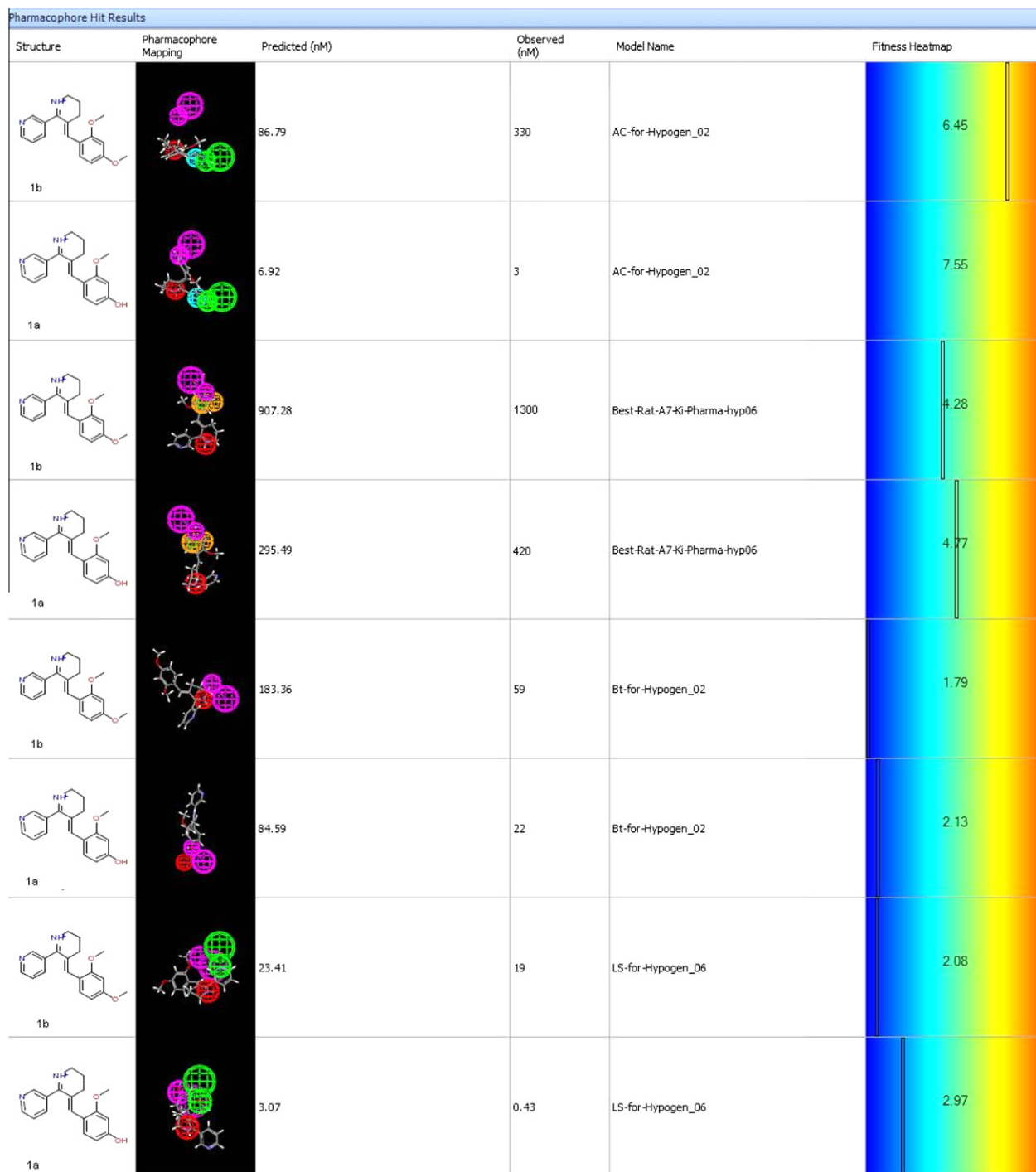


Figure 1. Heatmap of pharmacophore mapping & fitness for compounds **1a** and **1b**, derived from the best pharmacophore hypothesis obtained for rat $\alpha 7$ Ac, Bt, and Ls. Observed and predicted K_d values for AChBPs and K_i values for $\alpha 7$ nAChR are also shown. Chemical features are colored as follows: green: hydrogen bond acceptor, red: positive charge, magenta: hydrogen bond donor, and orange: aromatic ring.

for each ligand, the contribution of hydrophobic enclosures and pairwise lipophilic interactions derived from docking made about 50% of the total Glide score. This result suggests a strong contribution of hydrophobic interactions in the overall free energy of binding and is in agreement with the pharmacophore models obtained. Compound **3a** ($\alpha 7$ nAChR K_i 7.2 nM) exhibited better binding affinity for $\alpha 7$ than compounds **1b** ($\alpha 7$ nAChR K_i 1300 nM) and **1a** ($\alpha 7$ nAChR K_i 420 nM), and demonstrated partial agonism with an E_{max} of $53.0 \pm 4.4\%$ and an EC_{50} of $0.6 \pm 0.5 \mu M$, by patch-clamp electrophysiology in rat $\alpha 7$ nAChR. Compound **1a**

exhibits a longer HBD-cation distance (8.96 Å), in comparison to the designed actives counterparts (5.47–7.65 Å). By contrast, compounds **2h**, **3c**, **3e**, which have a HBD-cation distance within the shortest range of 3.52–4.72 Å, and thus lack a HBD that satisfies the required distance constraint, do not interact with $\alpha 7$ nAChR.

Further examination of Table 2 indicates that on the whole, designed compounds have a lower number of rotatable bonds (1–3), as compared to the parent compounds **1a** (4) and **1b** (4). This results in reduced ligand flexibility, which in turns would promote binding affinity due to loss of configurational entropy. Thus, in

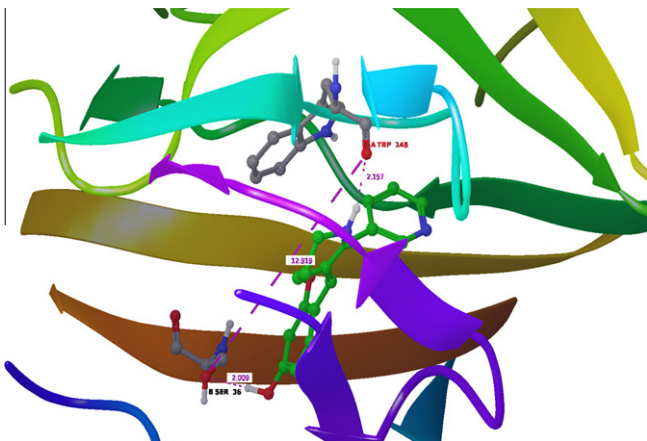


Figure 2a. Compound **1a** docked into rat $\alpha 7$ homology model, is shown in green. The ligand OH group donates a hydrogen-bond to Ser-36 (in the complementary face). The cationic center donates a hydrogen bond to the backbone CO group of Trp-148, in the principal face. Also shown are the hydrogen-bond donor to acceptor distances (2.00 and 2.15 Å) and the distance between the backbone oxygen atom of Trp-148 and side-chain oxygen atom of Ser-36 and Asp-164 (12.9 Å).

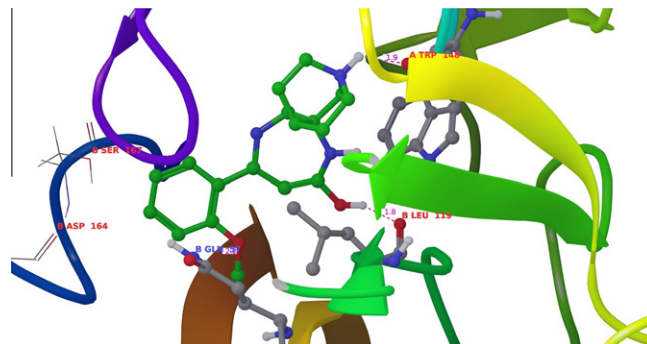


Figure 4a. Designed compound **2b** (in its lactim form) docked into rat $\alpha 7$ homology model, is shown in ball and stick and colored green. The ligand OH group donates a hydrogen-bond to the backbone carbonyl oxygen atom of Leu-119 (in the complementary face), while its methoxy group accepts a hydrogen bond from Gln-57 (in the complementary face). The cationic center donates a hydrogen-bond to the backbone CO group of Trp-148, in the principal face. Neighboring amino-acid side chains of the F-loop, such as Asp-164 and Ser-167, are shown in stick, while residues making hydrogen-bond with the ligand are shown in ball and stick.

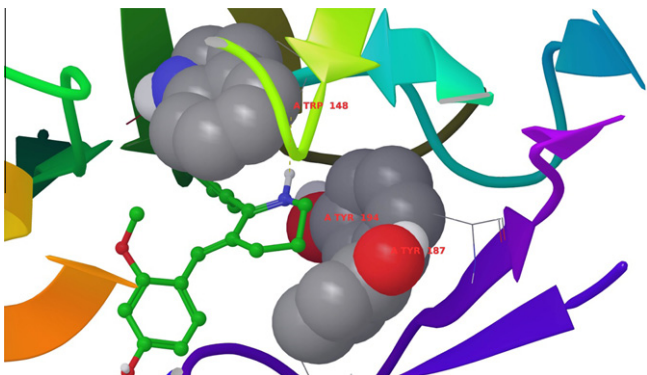


Figure 2b. Compound **1a** docked into rat $\alpha 7$ homology model, is shown in ball and stick and colored green. Trp-148, Tyr-187 and Tyr-194 (of the principal face) which are involved in cation- π interactions with the basic nitrogen of the ligand, are shown in space-filling representation.

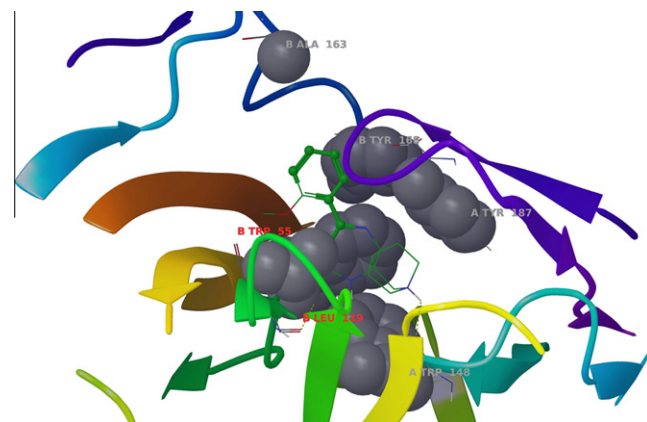


Figure 4b. Designed compound **2b** (in its lactim form) docked into rat $\alpha 7$ homology model, is shown in green. Trp-148, Tyr-187 (of the principal face), and Trp-55, Ala-163, Leu-119, and Tyr-168 (of the complementary face) which are involved in hydrophobic enclosures interactions with the ligand, are shown in space-filling representation. Portions of the ligand which are involved in hydrophobic enclosures are shown in ball and stick.

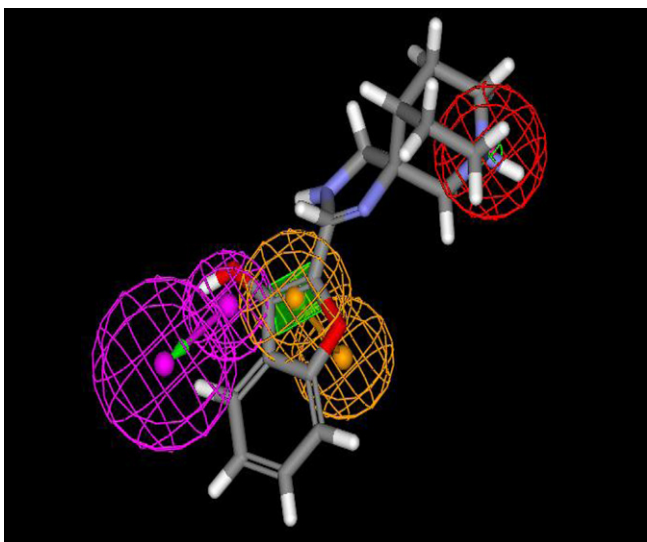


Figure 3. Pharmacophore mapping of designed compound **3a** onto the best pharmacophore hypothesis of rat $\alpha 7$. The positive charge, HBD and aromatic ring chemical features are shown in red, magenta and orange, respectively.

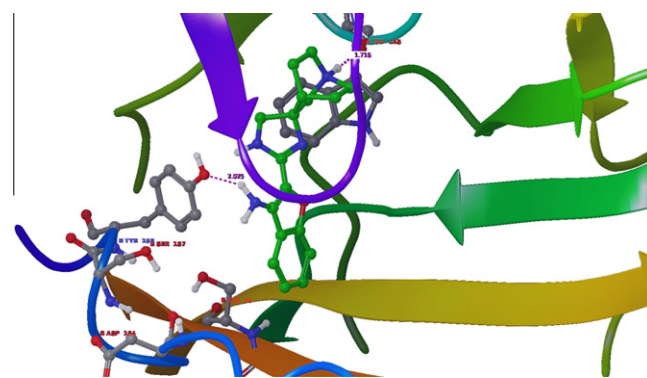
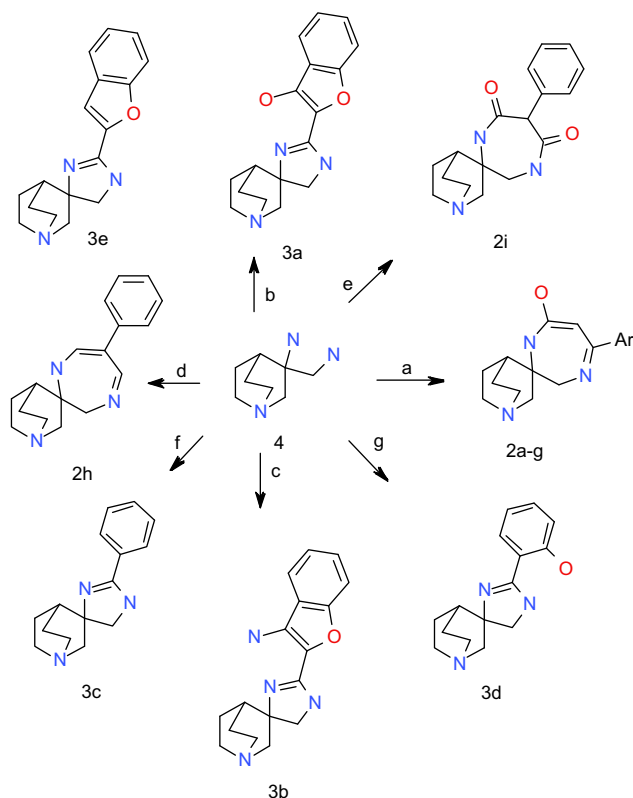


Figure 5. Designed compound **3b** docked into rat $\alpha 7$ homology model. The ligand OH group donates a hydrogen-bond to Tyr-168 (in the complementary face), which is located in the F-loop (shown in dark blue). Also shown are neighboring amino-acid side chains such as Ser-167, Asp-164, and Ser-36. The cationic center donates to the backbone CO group of Trp-148, in the principal face. Both hydrogen-bond distances are shown in broken lines.



Scheme 1. Synthesis of $\alpha\gamma$ nAChR ligands. Reagents and conditions: (a) $\text{ArCOCH}_2\text{CO}_2\text{Me}$, $i\text{-BuOH}$, 100°C , overnight; (b) methyl 2-(cyanomethyl)benzoate, CS_2 (one drop), $100\text{--}110^\circ\text{C}$, overnight; (c) (2-cyanophenoxy)acetonitrile, CS_2 (one drop), $100\text{--}110^\circ\text{C}$, overnight; (d) [3-(dimethylamino)-2-phenylprop-2-enylidene]dimethylammonium hexafluorophosphate, MeOH , reflux, overnight; (e) diethyl 2-phenylmalonate, 150°C , 5 min; (f) methyl benzimidate hydrochloride, methanol, 150°C (microwave), 5 min; (g) 4-hydroxycoumarin, $t\text{-butanol}$, 100°C , overnight.

addition to the proper spatial arrangement of the cationic center with respect to the hydrogen-bond donor group and hydrophobic aromatic group, ligand rigidity contributes to the increase in binding affinity of designed ligands, in comparison to GTS-21. **Figure 3**

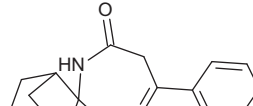
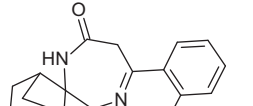
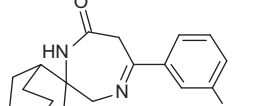
illustrates the mapping of compound **3a** onto the best pharmacophore of rat $\alpha 7$.

The binding modes of compounds **2b** and **3b** into the rat $\alpha 7$ protein binding site, as predicted via docking, are shown in Figures 4 and 5, respectively. Figure 4a shows that the OH group of the lactim form of compound **2b** donates a hydrogen-bond to Gln-57. The oxygen atom of its methoxy group, accepts a hydrogen-bond from the backbone NH group of Leu-119. This predicted binding mode is similar to the one experimentally-observed in the co-crystal structure of compound **1b** (conformation B) with AChBP.¹² Furthermore, Figure 4b shows that the designed ligand **2b** is involved in hydrophobic enclosures with both aliphatic and aromatic residues of both the principal and complementary faces. Similar pattern was also observed with other designed compounds. On the whole, designed compounds exhibited stronger cation- π and hydrophobic enclosures interactions than parent compounds **1a** and **1b**. Figure 5 shows that the NH₂ group of compound **3b** donates a hydrogen-bond to the OH group of Tyr-168, a residue located in the F-loop region. This predicted binding mode is similar to the one experimentally-observed in the co-crystal structure of compounds **1b** (conformation A) and **1a**, in complex with AChBP.¹²

A closer look at the rat $\alpha 7$ binding site suggests the existence of alternative homologous receptor-based pharmacophoric constraints which appear to be consistent with the type of interactions involving parent compounds and designed ligands described here in. As shown in [Figure 6](#), the side-chain oxygen atom of Gn-117, Tyr-168, Asn-77, Ser-36, Ser-34 and Ser-167 (of the complementary face) are separated from the main-chain carbonyl oxygen atom of the highly conserved Trp-148 (of the principal face) with a distance of about 10.3, 11.1, 11.3, 12.9, 13.9, and 14.7 Å, respectively. Likewise, a side-chain nitrogen atom of Arg-79 and Gln-57 (of the complementary face) is separated from the same oxygen atom of Trp-148 with a distance of 10.3 and 11.6 Å, respectively. Thus, side-chain heteroatoms of many amino acid residues surrounding the binding site of the rat $\alpha 7$ appear to be almost equidistantly located from the carbonyl oxygen atom of Trp-148, which is known to accept a quintessential hydrogen-bond donated by the cationic center, which in turn is engaged in cation- π interactions, as shown in [Figures 2 and 4](#). Such arrangement can accommodate diverse ligands and multiple binding modes.

Table 2

Table 2
Percent inhibition, \pm standard error, of control radioligand binding to nAChRs of the designed spirodiazepine and spiroimidazoline quinuclidines tested at 5 μ M in radioactive displacement assays

Compound	Structure	$\alpha 7$	$\alpha 4\beta 2$	$\alpha 3\beta 4$	$\alpha 1\beta\gamma\delta$	AlogP98	HBD-cation distance (Å)	NROT
2a		95 ± 3 [3] (140 ± 7 [3])	15 ± 1 [3]	NT	NT	0.54	5.47	2
2b		87 ± 3 [3] (110 [1])	7 ± 1 [3]	NT	NT	0.52	5.53	3
2c		93 ± 7 [3] (87 [1])	12 ± 1 [3]	NT	NT	0.52	5.59	3

(continued on next page)

Table 2 (continued)

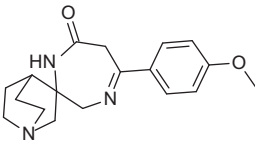
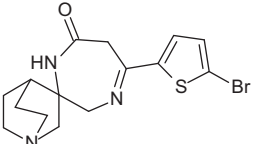
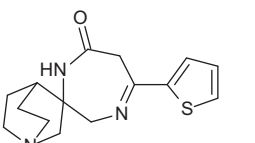
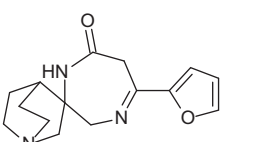
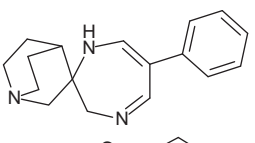
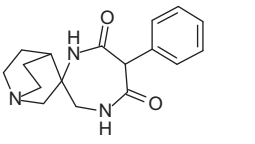
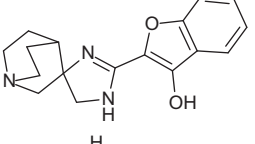
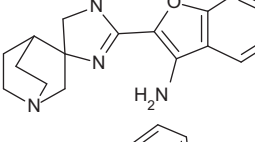
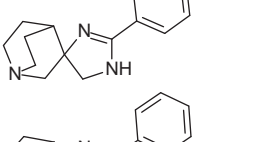
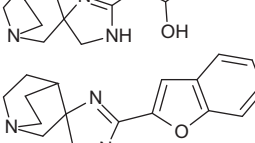
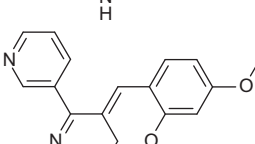
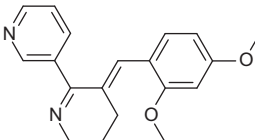
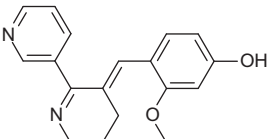
Compound	Structure	$\alpha 7$	$\alpha 4\beta 2$	$\alpha 3\beta 4$	$\alpha 1\beta\gamma\delta$	AlogP98	HBD-cation distance (Å)	NROT
2d		98 ± 3 [6] (42 [1])	42 ± 14 [6]	63 ± 0.4 [3]	38 ± 5 [3]	0.52	5.55	3
2e		95 ± 3 [6] (77 [1])	62 ± 15 [6]	89 ± 0.45 [3]	28 ± 6 [3]	1.25	5.61	2
2f		98 ± 2 [3] (58 [1])	20 ± 1 [3]	NT	NT	0.26	5.60	2
2g		84 ± 4 [3] (150 [1])	14 ± 3 [3]	NT	NT	−0.07	5.60	2
2h		27 ± 5 [3]	6 ± 2 [3]	NT	NT	−0.17	3.52	1
2i		19 ± 1 [3]	2 ± 1 [3]	NT	NT	−2.33; −3.74; −2.33	5.10; 5.46; 6.97; 6.15	2; 2; 3
3a		93 ± 6 [9] (7 ± 3 [4])	32 ± 11 [9]	55 ± 3 [6]	15 ± 10 [6]	0.30	5.75	2
3b		96 ± 1 [3] (120 [1])	9 ± 1 [3]	47 ± 3 [3]	38 ± 2 [3]	−0.20	7.65	1
3c		1 ± 9 [3]	11 ± 2 [3]	NT	NT	−0.05	4.64	1
3d		77 ± 3 [3] (290 [1])	4 ± 1 [3]	NT	NT	−0.29	5.62 ; 4.66	2
3e		33 ± 3 [3]	4 ± 2 [3]	13 ± 1 [3]	26 ± 5 [3]	0.54	4.72	1
1b		(1300 ± 550 [4])	(51 ± 10 [3])	(2500 ± 270 [3])	(3900 ± 770 [3])	3.03	NA	4

Table 2 (continued)

Compound	Structure	$\alpha 7$	$\alpha 4\beta 2$	$\alpha 3\beta 4$	$\alpha 1\beta\gamma\delta$	AlogP98	HBD-cation distance (Å)	NROT
1a		106 ± 3 [3] (420 [1])	97 ± 1 [3] (19 ± 6 [4])	75 ± 1 [3] (970 ± 110 [4])	72 ± 3 [3]	2.81	8.96	4

Values in parentheses represent $K_i \pm$ standard error in nM. The number of replicates is listed beside each result in brackets. The $\alpha 7$ radioligand [^3H]-methyllycaconitine was used for $\alpha 7$ binding studies on rat hippocampal membranes and the nicotinic radioligand [^3H]-epibatidine was used for binding studies at human $\alpha 4\beta 2$ heterologously expressed in SH-EP1 cells, ganglion-type nicotinic receptors on SH-SY5Y cellular membranes and muscle-type nicotinic receptors on TE-671 cellular membranes. See Experimental Section for details. NT = not tested. For comparison purpose, corresponding data for compounds **1a** and **1b** are also shown. The distance between the HBD and the cationic center for the lowest-energy conformation is also shown. For compound **2i**, the three plausible tautomeric forms are considered. The calculated partition coefficient between the organic and the aqueous phase expressed in terms of AlogP98, and the total number of rotatable bonds (NROT) for each compound, as derived from Pipeline Pilot (Accelrys Inc., San Diego, CA, 2006), are also listed.

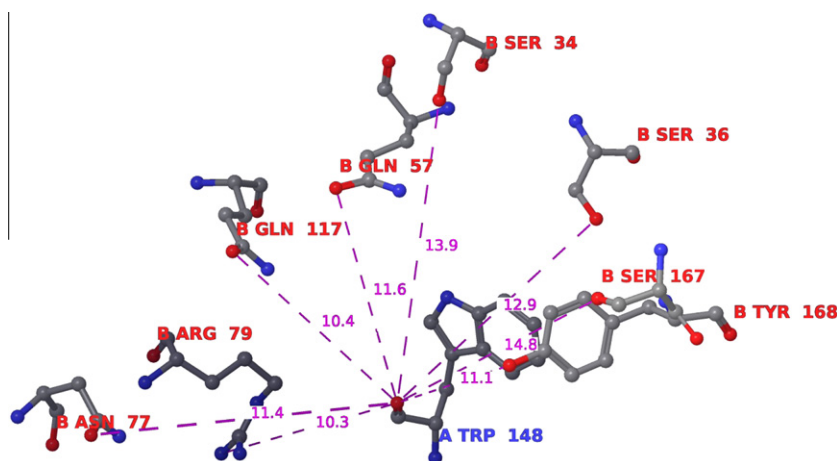


Figure 6. Conserved Trp-148 of the principal face and surrounding amino acid side-chains of the complementary face which are likely to interact with designed ligands. Also shown are the distances between the main chain carbonyl oxygen atom of Trp-148 and a side chain heteroatom of another amino acid residue.

However, our pharmacophore modeling and molecular docking studies described herein have neglected protein flexibility, and assumed that the protein is rigid. One may envision that due to molecular motions of the F-loop, side-chain oxygen atoms of Ser-166 and Asp-164, which are located at about 20.5 and 19.4 Å from the main chain carbonyl oxygen atom of Trp-148 in the homology model used herein, may reach a position closer to the conserved Trp residue, and thus meet the pharmacophoric requirement.

In conclusion, we have used pharmacophore elucidation and molecular docking to study the interactions of benzylidene anabaseine congeners with AChBPs and rat $\alpha 7$ nAChR. We have found that binding affinity is primarily mediated via electrostatic interactions (hydrogen-bond, π -cation and π - π) and hydrophobic interactions as well. In particular, a hydrogen bond donor feature appears to contribute to ligand binding to AChBPs and $\alpha 7$ nAChR. We have used this pharmacophore to design novel spirodiazepine and spiroimidazoline quinuclidine series. As predicted, docking-derived binding modes of these ligands are strikingly reminiscent of those observed in co-crystal structures of benzylidene anabaseine analogs with AChBP. Experimentally-observed data have shown that the designed compounds selectively bind to rat $\alpha 7$ nAChR. In particular, compound **3a** binds $\alpha 7$ nAChR with a much better affinity than both GTS-21 and its active metabolite, and demonstrates partial agonism. Our studies have also revealed the existence of alternative pharmacophoric features equidistant from the carbonyl oxygen atom of the conserved Trp-148 of the principal face, which may be exploited to design diverse focused libraries targeting the $\alpha 7$ nAChR.

Acknowledgments

We sincerely thank Dr. Gary Byrd for high resolution LCMS and Christopher Helper for binding affinity studies. We also thank Merouane Bencherif, Craig Miller, and Heather Savelle for helpful discussions, suggestions and comments.

References and notes

- Lippiello, P. M.; Bencherif, M.; Hauser, T. A.; Jordan, K. G.; Letchworth, S. R.; Mazurov, A. A. *Expert Opin. Drug Discov.* **2007**, *2*, 1185.
- Law, R. J.; Henschman, R. H.; McCammon, A. *Proc. Natl. Acad. Sci. U.S.A.* **2005**, *102*, 6813.
- Marks, M. J.; Collins, A. C. *Mol. Pharmacol.* **1982**, *3*, 554.
- Freedman, R.; Hall, M.; Adler, L. E.; Leonard, S. *Biol. Psychiatry* **1995**, *38*, 22.
- Bertrand, D.; Gopalakrishnan, M. *Biochem. Pharmacol.* **2007**, *74*, 1155.
- Freedman, R.; Coon, H.; Myles-Worsley, M.; Orr-Urtreger, A.; Olincy, A.; Davis, A.; Polymeropoulos, M.; Holil, J.; Hopkins, J.; Hoff, M.; Rosenthal, J.; Waldo, M. C.; Reimherr, F.; Wender, P.; Yaw, J.; Young, D. A.; Breese, C. R.; Adams, C.; Patterson, D.; Adler, L. E.; Kruglyak, L.; Leonard, S.; Byerley, W. *Proc. Natl. Acad. Sci. U.S.A.* **1997**, *94*, 587.
- Brejč, K.; van Dijk, W. J.; Klaassen, R. V.; Schurmans, M.; van de Oost, J.; Smit, A. B.; Sixma, T. K. *Nature* **2001**, *411*, 269.
- Unwin, N. *J. Mol. Biol.* **2005**, *346*, 967.
- Bourne, Y.; Talley, T. T.; Hansen, S. B.; Taylor, P.; Marchot, P. *EMBO J.* **2005**, *24*, 1512.
- Celie, P. H.; Rossum-Fikkert, S. E.; van Dijk, W. J.; Brejč, K.; Smit, A. B.; Sixma, T. K. *Neuron* **2004**, *41*, 907.
- Celie, P. H.; Klaassen, R. V.; Rossum-Fikkert, S. E.; van Elk, R.; van Nierop, P.; Smit, A. B.; Sixma, T. K. *J. Biol. Chem.* **2005**, *280*, 26457.
- Hibbs, R. E.; Sulzenbacher, G.; Shi, J.; Talley, T. T.; Conrod, S.; Kem, W. R.; Taylor, P.; Marchot, P.; Bourne, Y. *EMBO J.* **2009**, *28*, 3040.
- Mecozzi, S.; West, A. P.; Dougherty, D. A. *Proc. Natl. Acad. Sci. U.S.A.* **1996**, *93*, 10566.
- Schmitt, J. D.; Sharples, C. G.; Caldwell, W. S. *J. Med. Chem.* **1999**, *42*, 3066.

15. Dougherty, D. A. *J. Org. Chem.* **2008**, *16*, 3667.
16. Ulens, C.; Akdemir, A.; Jongejan, A.; van Elk, R.; Bertrand, S.; Perrakis, A.; Leurs, R.; Smit, A. B.; Sixma, T. K.; Bertrand, D.; de Esch, I. J. P. *J. Med. Chem.* **2009**, *52*, 2372.
17. Papke, R. L.; Meyer, E. M.; Lavieri, S.; Bollonally, S. R.; Papke, T. A.; Horenstein, N. A.; Itoh, Y.; Papke, J. K. *Neuropharmacology* **2004**, *46*, 1023.
18. Stokes, C.; Papke, J. K.; Horenstein, N. A.; Kem, W. R.; McCormack, T. J.; Papke, R. L. *Mol. Pharmacol.* **2004**, *66*, 14.
19. 3D-QSAR Pharmacophore models aimed at predicting ligand binding to AChBPs and rat $\alpha 7$ were built using the datasets described in ; Talley, T. T.; Yalda, S.; Ho, K.-Y.; Tor, Y.; Soti, F. S.; Kem, W. R.; Taylor, P. *Biochemistry* **2006**, *45*, 8894, and in ; Slavov, S. H.; Radzvilovits, M.; LeFrancois, S.; Stoyanova-Slavova, I.; Sot, F.; Kem, W. R.; Katritzky, A. R. *Eur. J. Med. Chem.* **2010**, *45*, 2433, respectively. The training sets used to build Ac, Bt, Ls, and rat $\alpha 7$ binding models were comprised of 21, 20, 20, and 20 compounds, respectively. In the later case, adopting their terminology, the ID of each benzylidene anabaseine analog selected to be included in the training set was: 1.1, 1.11, 1.13, 1.14, 1.15, 1.2, 1.22, 1.23, 1.26, 1.27, 1.3, 1.36, 1.37, 1.4, 1.41, 1.42, 1.43, 1.44, 1.45, 1.5, 1.6, 1.7, 1.8, and 1.9. Models were developed using Discovery Studio (Accelrys Inc., San Diego, CA, 2006). Variable weights to the chemical features were automatically assigned. Ligand conformational models were generated using the BEST option, with an energy cutoff of 20 kcal/mol and the maximum number of conformations set to 250. Fischer randomization test was used to demonstrate that derived models were not generated by chance, that is, that a true correlation exists between the biological activity and the structural features. Binding affinity prediction for designed ligands was carried out by computing pharmacophore hypothesis fitness values and K_d estimates using 'ligand pharmacophore mapping' module as implemented in Discovery Studio. Further validation of the $\alpha 7$ pharmacophore model was carried out by predicting a diverse library of 493 compounds, comprised of 127 actives ($\alpha 7$ $K_i \leq 500$ nM) and 366 decoys ($\alpha 7$ $K_i > 500$ nM). The performance of the model to rank these compounds with respect to their binding affinity, was evaluated by means of the area under the receiver operating characteristic (ROC) curve, and the enrichment curve. The ROC accuracy obtained was 0.62, and the enrichment factor of 1.75. If Yield designates the ratio of the number of actives recovered to the total hit list size, the enrichment is equal to Yield \times (D/A), where D is the total number of compounds in the dataset (493) and A the total number of active compounds in the dataset (127).
20. Docking studies were carried out using Glide 5.5 (Schrodinger, Inc., 101 SW Main Street, Suite 1300, Portland, OR 97204), as described in; Friesner, R. A.; Banks, J. L.; Murphy, R. B.; Halgren, T. A.; Klicic, J. J.; Mainz, D. T.; Repasky, M. P.; Knoll, E. H.; Shelley, M.; Perry, J. K.; Shaw, D. E.; Francis, P.; Shenkin, P. S. *J. Med. Chem.* **2004**, *47*, 1739; Halgren, T. A.; Murphy, R. B.; Friesner, R. A.; Beard, H. S.; Frye, L. L.; Pollard, W. T.; Banks, J. L. *J. Med. Chem.* **2004**, *47*, 1750. To validate the procedure, a self-docking of **1b** and its metabolite **1a** into their cognate Aplysia AChBP with the structure, obtained from Hibbs, R. E.; Sulzenbacher, G.; Shi, J.; Talley, T. T.; Conrod, S.; Kem, W. R.; Taylor, P.; Marchot, P.; Bourne, Y. *EMBO J.* **2009**, *28*, 3040, was carried. Glide-derived docked poses were within an average rmsd of 1.3 Å with respect to the native co-crystallized conformation. Homology models of the extracellular domain of rat $\alpha 7$ nAChR were obtained using MODELLER (Accelrys Inc., San Diego, CA, 2006), as described in Eswar, N.; Marti-Renom, M. A.; Webb, B.; Madhusudhan, M. S.; Eramian, D.; Shen, M.; Pieper, U.; Sali, A. Comparative Protein Structure Modeling With MODELLER. In *Current Protocols in Bioinformatics*, John Wiley & Sons; **2006**, Supplement 15, 5.6.1–5.6.30, 200; Marti-Renom, M. A.; Stuart, A.; Fiser, A.; Sánchez, R.; Melo, F.; Sali, A. *Annu. Rev. Biophys. Biomol. Struct.* **2000**, *29*, 291. The crystal structure of AChBP from *Ilymnaea* complexed with nicotine (pdb code 1uw6) was used as template. The derived protein models were validated using Procheck (Laskowski, R. A.; MacArthur, M. W.; Moss, D. S.; Thornton, J. M. *App. Cryst.* **1993**, *26*, 283) and Verify_3D (Eisenberg, D.; Luthy, R.; Bowie, J. U. *Methods Enzymol.* **1997**, *277*, 396). Further validation of the $\alpha 7$ model was carried out by docking a diverse library of 493 compounds, comprised of 127 actives ($\alpha 7$ $K_i \leq 500$ nM) and 366 decoys ($\alpha 7$ $K_i > 500$ nM). Glide performance to rank these compounds with respect to their binding affinity, was evaluated by means of the area under the receiver operating characteristic (ROC) curve. The accuracy obtained was 0.74.
21. Mullen, G.; Napier, J.; Balestra, M.; DeCory, T.; Hale, G.; Macor, J.; Mack, R.; Loch, J.; Wu, E.; Kover, A.; Verhoest, P.; Sampognaro, A.; Phillips, E.; Zhu, Y.; Murray, R.; Griffith, R.; Blosser, J.; Gurley, D.; Machulskis, A.; Zongrone, J.; Rosen, A.; Gordon, J. *J. Med. Chem.* **2000**, *43*, 4045.
22. 5-Phenylspiro[1,3-dihydro-1,4-diazepine-2,3'-quinuclidine]-7-ol (**2a**): This procedure illustrates the general method for preparation of **2a-g**. 3-Amino-3-(aminomethyl)quinuclidine (**1**) (75 mg, 0.5 mmol) and ethyl benzoylacetate (100 mg, 0.5 mmol) were dissolved in *i*-butanol (3 ml). The reaction mixture was heated at 100 °C overnight, cooled to ambient temperature and concentrated. The residue was purified by preparative HPLC to yield **2a** trifluoroacetate (105 mg, 53%). ¹H NMR (CD₃OD, 300 MHz) δ 8.07d (d, 2H), 7.72 (m, 1H), 7.60 (m, 2H), 4.23 (dd, 2H, J = 65, 12 Hz), 3.94 (dd, 2H, J = 28, 10 Hz), 3.59–3.38 (m, 6H), 2.49 (s, 1H), 2.35–2.10 (m, 4H). High resolution LSMS, m/e 284.1767, C₁₇H₂₂N₃O, calcd 284.1763.
- 6-Phenylspiro[1,3-dihydro-1,4-diazepine-2,3'-quinuclidine] (**2h**): 3-Amino-3-(aminomethyl)quinuclidine (**1**) (75 mg, 0.5 mmol) and [3-(dimethylamino)-2-phenylprop-2-enylidene]-dimethylammonium hexafluorophosphate (100 mg, 0.4 mmol) were dissolved in methanol (5 ml). The reaction mixture was refluxed overnight and concentrated. The residue was purified by preparative HPLC to yield **2h** trifluoroacetate (75 mg (20%). ¹H NMR (CD₃OD, 300 MHz) δ 0.15 (s, 1H), 8.01 (s, 1H), 7.52–7.38 (m, 5H), 4.50 (d, 1H, J = 12 Hz), 3.73 (dd, 2H, J = 27, 12 Hz), 3.60–3.38 (m, 5H), 2.22–1.98 (m, 5H).
- 6-Phenylspiro[1,4-diazepane-2,3'-quinuclidine]-5,7-dione (**2i**): A mixture of 3-amino-3-(aminomethyl)quinuclidine (**1**) (75 mg, 0.5 mmol) and diethyl 2-phenylmalonate (118 mg, 0.5 mmol) were heated at 150 °C in microwave for 5 min. The reaction mixture was cooled to rt and purified by preparative HPLC to yield **2i** trifluoroacetate (98 mg, 24%). ¹H NMR (CD₃OD, 300 MHz) δ 7.46–7.22 (m, 5H), 4.30 (s, 1H), 4.02 (dd, 2H, J = 50, 13 Hz), 3.53 (dd, 2H, J = 53, 12 Hz), 3.53–3.15 (m, 4H), 2.23–1.98 (m, 5H). High resolution LCMS m/e 300.1723, C₁₇H₂₂N₃O₂, calcd 300.1712.
- 2-(3-Hydroxybenzofuran-2-yl)spiro[1,5-dihydroimidazole-4,3'-quinuclidine] (**3a**): A mixture of 3-amino-3-(aminomethyl)quinuclidine (**1**) (75 mg, 0.5 mmol), methyl 2-(cyanomethoxy)benzoate (96 mg, 0.5 mmol) and one drop of carbon disulfide was heated in a sealed vial at 100–110 °C overnight. The reaction mixture was cooled to rt and purified by preparative HPLC to yield **3a** trifluoroacetate (98 mg, 48%). ¹H NMR (CD₃OD, 300 MHz) δ 7.98 (d, 1H), 7.65 (m, 2H), 7.43 (m, 2H), 4.26 (dd, 2H, J = 76, 12), 3.77 (dd, 2H, J = 35, 14), 3.60–3.38 (m, 4H), 2.50–2.33 (m, 2H), 2.15 (m, 3H).
- 2-(3-Aminobenzofuran-2-yl)spiro[1,5-dihydroimidazole-4,3'-quinuclidine] (**3b**): A mixture of 3-amino-3-(aminomethyl)quinuclidine (**1**) (75 mg, 0.5 mmol), (2-cyanophenoxy)acetonitrile (79 mg, 0.5 mmol) and one drop of carbon disulfide was heated in a sealed vial at 100–110 °C overnight. The reaction mixture was cooled to rt and purified by preparative HPLC to yield **3b** trifluoroacetate (145 mg, 68%). ¹H NMR (CD₃OD, 300 MHz) δ 7.96 (d, 1H), 7.64 (t, 1H), 7.50 (d, 1H), 7.36 (t, 1H), 4.20 (dd, 2H, J = 60, 12 Hz, 2H), 3.79 (dd, 2H, J = 22, 12 Hz, 2H), 3.63–3.38 (m, 4H), 2.42 (m, 2H), 2.17 (m, 3H). High resolution LCMS m/e 290.1707, C₁₇H₂₁N₄O, calcd 290.1715.
- 2-Phenylspiro[1,5-dihydroimidazole-4,3'-quinuclidine] (**3c**): A mixture of 3-amino-3-(aminomethyl)quinuclidine (**1**) (475 mg, 3.0 mmol) and methyl benzimidate hydrochloride (602 mg, 3.5 mmol) in methanol (3 ml) was heated in microwave at 150 °C for 5 min. The reaction mixture was concentrated in vacuo. The residue was purified by preparative HPLC to yield **3c** (0.3 g, 28%). ¹H NMR (CD₃OD, 300 MHz) δ 8.00 (d, 2H), 7.85 (m, 1H), 7.69 (m, 2H), 4.33 (dd, 2H, J = 75, 11), 3.80 (dd, 2H), 3.59–3.37 (m, 4H), 2.59–2.40 (m, 2H), 2.09 (m, 3H). High resolution LCMS m/e 242.1649, C₁₅H₂₀N₃, calcd 242.1657.
- 2-Spiro[1,5-dihydroimidazole-4,3'-quinuclidine]-2-ylphenol (**3d**): 3-Amino-3-(aminomethyl)quinuclidine (**1**) (75 mg, 0.5 mmol) and 4-hydroxycoumarin (81 mg, 0.5 mmol) were dissolved in *i*-butanol (3 ml). The reaction mixture was heated at 100 °C overnight, cooled to ambient temperature and concentrated. The residue was purified by preparative HPLC to yield **3d** trifluoroacetate (15 mg, 8%). ¹H NMR (CD₃OD, 300 MHz) δ 7.88 (d, 1H), 7.66 (m, 1H), 7.12 (m, 2H), 4.29 (dd, 2H, J = 79, 10), 4.78 (dd, 2H), 3.56–3.37 (m, 4H), 2.50–2.33 (m, 2H), 2.16 (m, 3H).
23. Binding assays to membrane bound nicotinic receptors were carried out using standard methods adapted from published procedures, for example, Lippello, P. M.; Fernandes, K. G. *Mol. Pharmacol.* **1986**, *29*, 448; Davies, A. R.; Hardick, D. J.; Blagbrough, I. S.; Potter, B. V.; Wolstenholme, A. J.; Wonnacott, S. *Neuropharmacology* **1999**, *38*, 679. Single-point binding data was determined at a competitor concentration of 5 μ M and are expressed as the percent inhibition of control radioligand binding. For IC₅₀ determinations, replicates for each point of a seven-point dose-response curve were averaged and plotted against the log of drug concentration. IC₅₀ values (concentration of the compound that produces 50% inhibition of binding) were determined by least squares non-linear regression using GraphPad Prism software (GraphPAD, San Diego, CA). K_i values were calculated using the Cheng–Prusoff equation, Cheng, Y.; Prusoff, W. H. *Biochem. Pharmacol.* **1973**, *22*, 3099.
24. (a) Puodzhyunaite, B. A.; Yanchene, R. A.; Terent'ev, P. B. *Chem. Heterocycl. Compd.* **1988**, *16*, 311; (b) Andronati, S. A.; Yur'eva, V. S.; Mazurov, A. A.; Nivorozhkin, L. E. *Chem. Heterocycl. Compd.* **1984**, *20*, 451.